

CERN-EP-2025-086
07 April 2025

Spectroscopy of Strange Mesons and First Observation of a Strange Crypto-Exotic State with $J^P = 0^-$

The COMPASS Collaboration

Abstract

We measured the strange-meson spectrum in the scattering reaction $K^- + p \rightarrow K^- \pi^- \pi^+ + p$ with the COMPASS spectrometer at CERN. Using the world's largest sample of this reaction, we performed a comprehensive partial-wave analysis of the mesonic final state. It substantially extends the strange-meson spectrum covering twelve states with masses up to $2.4 \text{ GeV}/c^2$. We observe the first candidate for a crypto-exotic strange meson with $J^P = 0^-$ and find K_3 and K_4 states consistent with predictions for the ground states.

(to be submitted to Phys. Rev. Letters)

I Introduction

Our knowledge and understanding of strongly bound systems of quarks and anti-quarks is mostly limited to non-strange light and to heavy hadrons. Strange mesons are only poorly known and dedicated theoretical studies are limited, but are necessary to bridge the gap between light and heavy hadrons. At present, 17 strange mesons are experimentally established (see PDG [1] and Fig. 1). Eight other states need confirmation, most of them observed by only a single experiment and in only a single decay channel. Models using constituent quarks and SU(3) flavor symmetry provide a pattern of $q\bar{q}'$ states [3–7] (black horizontal lines in Fig. 1). However, many of the predicted states are still unobserved. They are challenging to identify experimentally due to the dense strange-meson spectrum, e.g. caused by the fact that K_J states appear as pairs close in mass, arising from the singlet and triplet $q\bar{q}'$ states.

In recent years, the study of meson spectra has revealed many exotic phenomena beyond $q\bar{q}'$ states. For example, four-quark states containing heavy quarks have been discovered, e.g. Ref. [8], and $\pi_1(1600)$, a candidate for a light hybrid meson, has been firmly established [9]. There is no evidence yet for strange counterparts, but the $K_0^*(700)/\kappa$ that is discussed as a four-quark state [10]. While some exotic non-strange light and heavy mesons are clearly identified by their non- $q\bar{q}'$ quantum numbers, in the strange sector no such model-independent observable exists that distinguishes quark-model from exotic states. Therefore, strange exotics can only be observed as additional states within the already dense spectrum of predicted $q\bar{q}'$ states. Consequently, these states are called supernumerary or crypto-exotic. To establish such states, it is necessary to map out the strange-meson excitation spectrum over a wide mass range.

In this paper, we present the strange-meson spectrum observed in the diffractive scattering reaction $K^- + p \rightarrow K^- \pi^- \pi^+ + p$ with the COMPASS spectrometer at CERN. We performed a partial-wave analysis, from which we obtained the masses and widths of eleven strange-meson resonances with masses up to $2.4 \text{ GeV}/c^2$. Details of this analysis can be found in Ref. [11].

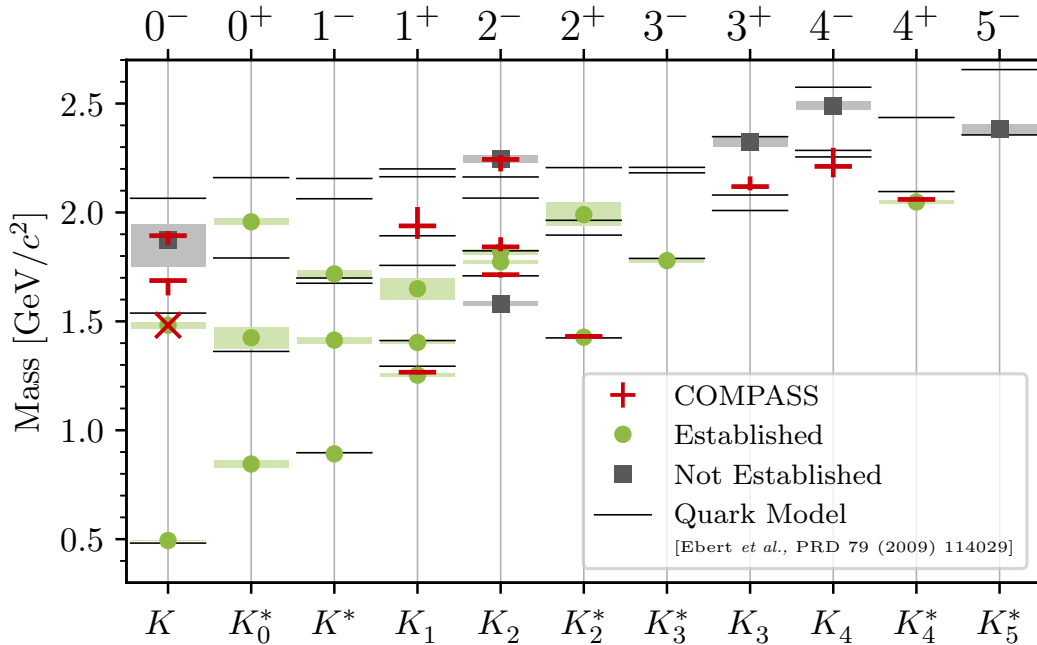


FIG. 1: Mass spectrum of strange mesons grouped by J^P quantum numbers (columns). Red horizontal lines represent our measurements, where the vertical lines indicate the total uncertainties on the mass. The red crosses represents our observation of the $K(1460)$, whose mass and width parameters were fixed to the LHCb measurement in Ref. [2]. Green points show established states; gray squares not established ones [1]. The box heights indicate the mass uncertainties. Black horizontal lines represent the quark-model calculation from Ref. [3].

II Method

The 190 GeV/c M2 beam at CERN contains about 2% K^- , which were identified by two differential Cherenkov counters. The $K^-\pi^-\pi^+$ final-state particles were measured with the COMPASS magnetic spectrometer and identified with a ring-imaging Cherenkov detector [12]. We imposed energy-momentum conservation and required that the reconstructed scattering vertex formed by all particles is inside the target volume. In total, our $K^-\pi^-\pi^+$ sample consists of 720000 exclusive events, exceeding the best previous measurement [13] by a factor of 3.6.

We performed a partial-wave analysis in two stages to identify spin and parity of strange mesons decaying into $K^-\pi^-\pi^+$ and to extract their masses and widths analogously to our work in Refs. [14, 15]. First, we determined the contributions of partial waves to the measured spectrum in terms of the spin-density matrix ρ_{ab} . To avoid making assumptions about the resonance content of the $K^-\pi^-\pi^+$ system at this stage, we independently determined $\rho_{ab}(m_{K\pi\pi}, t')$ in narrow bins of $m_{K\pi\pi}$ and four bins of the reduced four-momentum transfer squared t' between the beam kaon and the target proton in the ranges of $1.0 \text{ GeV}/c^2 \leq m_{K\pi\pi} < 3.0 \text{ GeV}/c^2$ and $0.1 (\text{GeV}/c)^2 \leq t' < 1.0 (\text{GeV}/c)^2$. To this end, the distribution of $K^-\pi^-\pi^+$ events in the phase-space variables τ in an $(m_{K\pi\pi}, t')$ bin was modeled as

$$I(\tau) = \sum_{a,b}^{\text{waves}} \psi_a(\tau) \rho_{ab} \psi_b^*(\tau). \quad (1)$$

Partial waves are labeled by $a = J^P M^\varepsilon \zeta \xi L$, where J^P are spin and parity, and M^ε is the spin projection along the beam axis expressed in the reflectivity basis [16]. We assume that the $K^-\pi^-\pi^+$ final state results from subsequent two-body decays via an intermediate isobar ζ , i.e. a two-body resonance. L is the orbital angular momentum between the bachelor particle ξ , which is a pion or a kaon, and the isobar. The decay amplitudes ψ_a are computed using the isobar model (see Refs. [17–19]). To infer the waves included in $\sum_{a,b}^{\text{waves}}$ that contribute significantly to the data, we use regularization-based model-selection techniques described in Ref. [11] to reduce the large pool of 596 allowed waves constructed using the loose constraints $J \leq 7$; $L \leq 7$; $M = 0, 1, 2$; $\varepsilon = +$; and a total of twelve isobar resonances in the $K^-\pi^+$ and $\pi^-\pi^+$ subsystems listed in Tab. 5.2 of Ref. [11]. Isobar resonances are parameterized by relativistic Breit-Wigner amplitudes [20], but special parameterizations from Refs. [14, 21, 22] and Ref. [23] are used for low-mass $\pi\pi$ and $K\pi$ S -wave isobars, respectively. We obtain $\rho_{ab}(m_{K\pi\pi}, t')$ by performing unbinned extended maximum-likelihood fits of Eq. (1) to the data, accounting for experimental acceptance. The statistical uncertainties are estimated by Bootstrapping [24], i.e. by randomly resampling and refitting the data sample.

Besides signal events, several backgrounds from other reactions, e.g. from $\pi^- + p \rightarrow \pi^-\pi^-\pi^+ + p$ caused by misidentified pions, leak into the $K^-\pi^-\pi^+$ sample. All backgrounds are accounted for by parameterizing ρ_{ab} as a matrix of rank three [11]. This effectively decomposes their intensity distribution into the $K^-\pi^-\pi^+$ partial-wave basis and adds them incoherently in Eq. (1).

In the second stage, we performed a resonance-model fit (RMF) to the measured $\rho_{ab}(m_{K\pi\pi}, t')$, to extract resonance signals from the partial waves and to determine their masses and widths. We selected 14 partial waves with signals covering almost all J^P in Fig. 1 (Table II in the supplemental material [25]) and modeled the corresponding $\rho_{ab}(m_{K\pi\pi}, t')$ as a sum over true $K^-\pi^-\pi^+$ and two incoherent background contributions, i.e.

$$\rho_{ab} = \mathcal{T}_a \mathcal{T}_b^* + \rho_{ab}^{3\pi} + \rho_{ab}^{\text{rem bkg}}, \quad (2)$$

where $\rho_{ab}^{3\pi}$ is a fixed parameterization for the largest incoherent background from $\pi^- + p \rightarrow \pi^-\pi^-\pi^+ + p$, which we determined from our own high-precision $\pi^-\pi^-\pi^+$ data [14], and $\rho_{ab}^{\text{rem bkg}}$ effectively subsumes

other remaining incoherent backgrounds by an adapted resonanceless parameterization (see Ref. [25] for details).

The true $K^- \pi^- \pi^+$ amplitudes are modeled as

$$\mathcal{T}_a(m_{K\pi\pi}, t') = \mathcal{K}(m_{K\pi\pi}, t') \sum_k C_a^k(t') \mathcal{D}_k(m_{K\pi\pi}), \quad (3)$$

which is a coherent sum over all model components k for the wave a . These include resonances and non-resonant components that account for multi-Regge processes [26, 27]. The dynamic amplitudes $\mathcal{D}_k(m_{K\pi\pi})$ of the resonance components are parameterized by relativistic Breit-Wigner functions, those of the non-resonant components by an empirical real-valued function (see Ref. [25]). $C_a^k(t')$ is the coupling amplitude of component k within the wave a , and is an independent constant for each t' bin. $\mathcal{K}(m_{K\pi\pi}, t')$ accounts for the phase-space volume and encodes the mass-dependent production by Pomeron exchange [28].

The $C_a^k(t')$ and shape parameters of $\mathcal{D}_k(m_{K\pi\pi})$, including e.g. the masses and widths, were determined by a χ^2 fit to the spin-density matrix elements of the 14 waves, taking into account their statistical correlations. These elements comprise 14 partial-wave intensities and 91 complex-valued interference terms. We performed extensive studies in order to estimate the systematic uncertainties of measured masses and widths (see section B in Ref. [25] for details).

III Ambiguous Identification of Final-State Particles

At COMPASS, the identification of final-state kaons and pions is limited to momenta below about 50 GeV/c. Events for which the identification was thus ambiguous were discarded from the analysis. This ambiguous identification renders a subset of partial waves indistinguishable for masses below about 1.6 GeV/c². They are therefore excluded from physics analysis. However, the 14 waves used in the resonance-model fit are interpretable, allowing us to extract strange mesons from them. This was confirmed in several systematic studies including extensive Monte Carlo input-output comparisons.

TABLE I: Our resonance parameters. The first quoted uncertainties are statistical, the second systematic.

Resonance	m_0 [MeV/c ²]	Γ_0 [MeV/c ²]
$K(1690)$	$1687 \pm 10^{+2}_{-67}$	$140 \pm 20^{+50}_{-50}$
$K(1830)$	$1893 \pm 17^{+13}_{-39}$	$160 \pm 40^{+60}_{-80}$
$K_1(1270)$	$1266 \pm 2^{+5}_{-9}$	$88 \pm 4^{+19}_{-19}$
K'_1	$1940 \pm 10^{+90}_{-60}$	$430 \pm 20^{+160}_{-190}$
$K_2(1770)$	$1714 \pm 4^{+10}_{-13}$	$152 \pm 8^{+78}_{-12}$
$K_2(1820)$	$1842 \pm 5^{+44}_{-19}$	$273 \pm 10^{+128}_{-22}$
$K_2(2250)$	$2244 \pm 10^{+18}_{-54}$	$260 \pm 20^{+50}_{-70}$
$K_2^*(1430)$	$1430.9 \pm 1.4^{+3.1}_{-1.5}$	$111 \pm 3^{+4}_{-16}$
K_3	$2119 \pm 13^{+45}_{-12}$	$270 \pm 30^{+40}_{-30}$
K_4	$2210 \pm 40^{+80}_{-30}$	$250 \pm 70^{+50}_{-70}$
$K_4^*(2045)$	$2060 \pm 5^{+11}_{-3}$	$189 \pm 10^{+13}_{-21}$

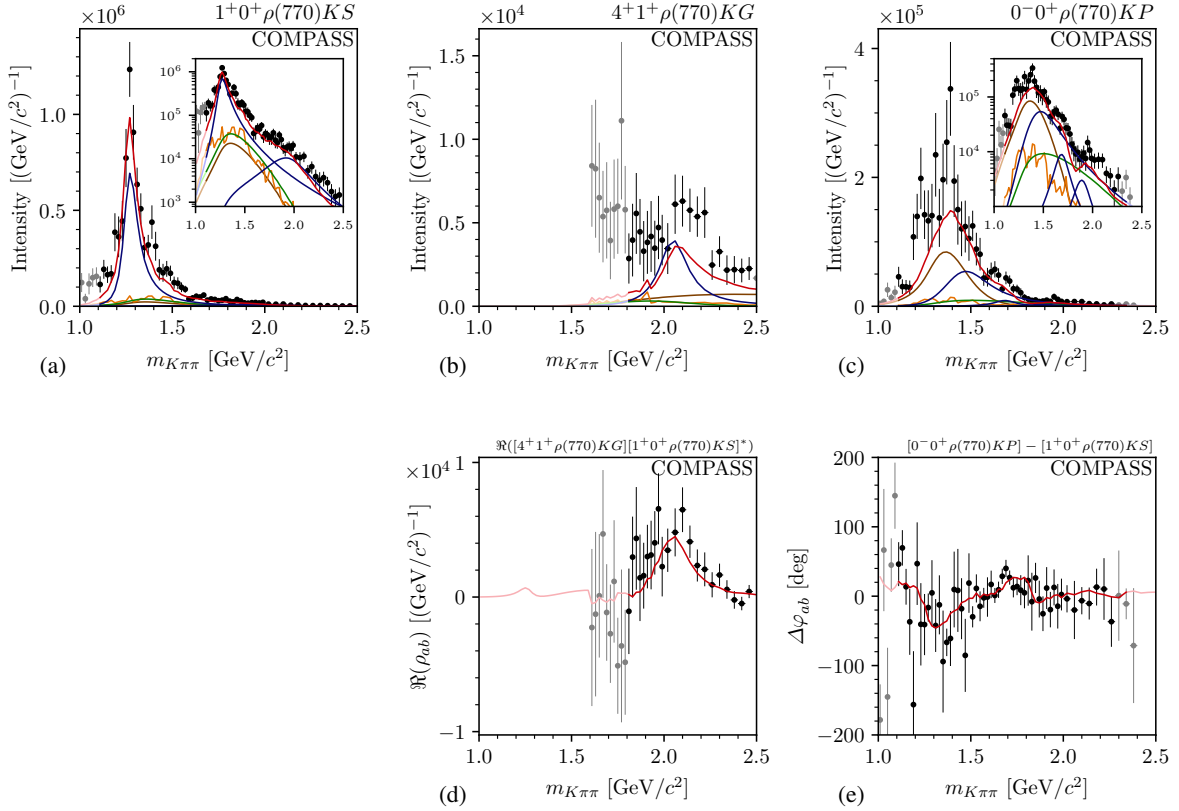


FIG. 2: Top row: intensity spectra of selected partial waves. Bottom row: real part $\Re(\rho_{ab})$ of the $4^+ 1^+ \rho(770)KG$ wave (d), and phase of the $0^- 0^+ \rho(770)KP$ wave (e), both relative to the $1^+ 0^+ \rho(770)KS$ wave. Data points represent the measurements. Curves represent the **total RMF model** (red), the individual **resonance components** (blue), the **non-resonant components** (green), the **$\pi^- \pi^- \pi^+$ background components** (orange), and the **remaining background components** (brown). Extrapolations of the model curves beyond fitted $m_{K\pi\pi}$ ranges are shown in lighter colors, grey for data points. The inserts in (a) and (c) show the intensity spectrum in log scale. All figures show the range of $0.1 (\text{GeV}/c)^2 \leq t' < 0.15 (\text{GeV}/c)^2$.

IV Results

Overall, the resonance-model fit reproduces well the spin-density matrix elements of the 14 selected waves as illustrated exemplarily in Fig. 2(a). The result for all spin-density matrix elements can be found in Figs. 3–9 of Ref. [25]. Table I lists the parameters of the eleven measured resonances, which we discuss below, starting with established states.

A Established K_1 and K_2^* States

Our $K_1(1270)$ width agrees well with the PDG average. Although our $K_1(1270)$ mass is slightly larger than the PDG average it is still consistent with it and also with several previous measurements [2, 13, 29, 30] and with a phenomenological model assuming a two-pole structure of the $K_1(1270)$ [31]. We do not observe a significant $K_1(1400)$ signal in the selected $J^P = 1^+$ waves. This is expected, since the ambiguous identification discussed above limits the analysis to the $\rho(770)K$ decay and the $K_1(1400)$ has a small branching fraction of this decay [1], which is at our detection limits.

In the mass range from 1.7 to 1.9 GeV/c^2 , quark models predict two excited K_1 states. However, the stability of the RMF allowed only a single excited K_1 Breit-Wigner component dubbed K_1' . LHCb reported two excited K_1 in the decay $B^+ \rightarrow J/\psi \phi K^+$ [8]. The parameters of the heavier of these two

states agree well with our K_1' signal. The PDG lists only a single excited K_1 called $K_1(1650)$. The PDG mass estimate is based on only a single measurement [32] and is much smaller than the mass of our signal and of the two states observed by LHCb.

Our $K_2^*(1430)$ mass and width agree well with the PDG averages. The corresponding uncertainties are competitive with previous measurements of the $K_2^*(1430)$.

B Ground and Excited K_2 States

Quark models predict two K_2 ground states in the $1.7 \text{ GeV}/c^2$ mass region. However, most previous experiments have identified only a single state. Only our measurement and previous measurements by LHCb [33] and LASS [34] could resolve two states, $K_2(1770)$ and $K_2(1820)$. LHCb data favor the 2-state hypothesis with a significance of 5.8σ . Our measurement yields an even higher statistical significance of 11σ , estimated from the χ^2 difference with respect to the single-resonance hypothesis using Wilks' theorem [35]. This clearly excludes the single-resonance hypothesis. Our resonance parameters agree well with both previous measurements, except for the $K_2(1770)$ mass, which is consistent with LHCb, but significantly lower than the LASS result. However, it is not clear whether the uncertainties of the LASS measurement include systematic effects. For the excited K_2 , our $K_2(2250)$ mass and width agree with the corresponding PDG average values, which are based only on analyses of $\Lambda \bar{p} / \bar{\Lambda} p$ final states. Our simultaneous measurement of three K_2 resonances with masses below and above $2 \text{ GeV}/c^2$ from the simultaneous fit to four partial waves representing the $K_2^*(1430)\pi$, $f_2(1270)K$, $K^*(892)\pi$, and $\rho(770)K$ decays is the most comprehensive single analysis of the strange $J^P = 2^-$ sector.

C K_3 and K_4 States

We measure the masses of a K_3 and a K_4 state, both in good agreement with quark-model predictions for the K_3 and K_4 ground states [3–7] (see Fig. 1). The only K_3 and K_4 states listed by the PDG are $K_3(2320)$ and $K_4(2500)$. Both have only been observed in the $\Lambda \bar{p} / \bar{\Lambda} p$ decay, the $K_3(2320)$ by the CERN Ω spectrometer [36] and the Geneva-Lausanne spectrometer [37], the $K_4(2500)$ by the latter one only [37]. However, the PDG masses for the $K_3(2320)$ and $K_4(2500)$ are about $200 \text{ MeV}/c^2$ larger than the masses of our K_3 and K_4 signals, and match better with quark-model predictions for the corresponding first excited states. This suggests that we have identified the K_3 and K_4 ground states, while the previous measurements may have observed the corresponding first excitations.

D Established $K_4^*(2045)$ State

Our measurements of the $K_4^*(2045)$ mass and width are the most accurate and agree with the PDG averages. The corresponding off-diagonal elements of ρ_{ab} are well reproduced (Fig. 2(d)). Our RMF reproduces the shape of the intensity given by ρ_{aa} fairly well, but underestimates it, as shown in Fig. 2(b). This is observed for several waves with relative intensities at the per mil level. The off-diagonal elements of ρ_{ab} representing interference with large waves are well constrained by data and encode information about the magnitude and phase of the partial wave. The measured intensities of small waves, however, are more weakly constrained as they contribute less to the modeled distribution of events in Eq. (1). As a result, the intensities are susceptible to analysis artifacts, e.g. caused by the ambiguous identification mentioned above.

The RMF is mainly driven by the off-diagonal ρ_{ab} elements, which are fit well. We therefore conclude that any potential bias in the resonance parameters from underestimating the intensities is small and covered by the quoted systematic uncertainties. The accurate measurement of the well-known $K_4^*(2045)$ and its robustness in systematic studies demonstrates our sensitivity to signals at the per mil level, despite the imperfections in modeling their intensity, and thus validates our analysis results.

E First Observation of a Crypto-Exotic $J^P = 0^-$ State

Excited pseudoscalar strange mesons are best seen in our $0^- 0^+ \rho(770) K P$ wave shown in Fig. 2(c). We observe three resonance structures with masses around $1.4 \text{ GeV}/c^2$, $1.7 \text{ GeV}/c^2$, and $1.9 \text{ GeV}/c^2$. The low-mass region of $m_{K\pi\pi} \lesssim 1.5 \text{ GeV}/c^2$ in this wave is weakly affected by the ambiguous identification discussed above. We therefore fixed the resonance parameters of the $K(1460)$ to the values obtained by LHCb [2], the measurement with smallest uncertainties.

Above the $K(1460)$, the pronounced peak at $1.7 \text{ GeV}/c^2$ is accompanied by a rise of the relative phase of the $0^- 0^+ \rho(770) K P$ wave, exemplarily shown in Fig. 2(e). The intensities and phases are well reproduced by a resonance component dubbed $K(1690)$. Again, we attribute imperfections in modeling the intensity to effects discussed above for the $J^P = 4^+$ waves. We estimated the statistical significance of the $K(1690)$ to be about 8σ .

A $K(1630)$ has been claimed by Refs. [38, 39] using bubble-chamber data on the reaction $\pi^- p \rightarrow (K_S^0 \pi^+ \pi^-) X^+ \pi^- X^0$ without performing a partial-wave analysis. Consequently, the authors did not determine the quantum numbers of their signal. To extract a peak, kinematic cuts had been applied restricting the phase space of the selected events without further justification. The reported width of $(16^{+19}_{-16}) \text{ MeV}/c^2$ is unusually small. Thus we do not consider their observation in the context of our $K(1690)$.

The RMF also yields the $K(1830)$, which corresponds to the small intensity bump at $1.9 \text{ GeV}/c^2$. The statistical significance is about 5σ . LHCb [33] has reported evidence for a similar signal, but our resonance parameters are more than twice as precise.

In total, our $0^- 0^+ \rho(770) K P$ wave exhibits evidence for three resonances signals. We identified these three signals in a single self-consistent analysis, fixing the lightest of the states to the values reported by LHCb. The significance of our observations and the measured resonance parameters are robust to all systematic studies. The presence of three states does not match quark-model predictions of only two states in this mass region [3–7]. This indicates the presence of a supernumerary signal. The lighter of the two quark-model states is consistent with the $K(1460)$, the heavier matches best the $K(1830)$. This leaves our observation of a $K(1690)$ as the first clear candidate for a crypto-exotic strange meson with $J^P = 0^-$. One should note that the observed states may be mixtures of pure quark-model and exotic states, and that a resonance-like structure, i.e. an intensity peak accompanied by a rising phase, can also be caused by kinematic singularities, including triangle singularities [40, 41].

V Conclusions

Our detailed and self-consistent partial-wave analysis of the world's largest data sample of the reaction $K^- + p \rightarrow K^- \pi^- \pi^+ + p$ yields the masses and widths of eleven strange-meson resonances in the mass region from 1.2 to $2.4 \text{ GeV}/c^2$. This is the most complete measurement of the strange-meson spectrum from a single analysis. We improve the resonance parameters for many states, in particular for the $K(1830)$. Our results also suggest that we have uncovered the K_3 and K_4 ground states for the first time. Most notably, we have identified the $K(1690)$, a supernumerary pseudoscalar resonance signal with a mass of about $1.7 \text{ GeV}/c^2$. This signal lies in mass between the two predicted quark-model states, which we also observe, and is the first candidate for a crypto-exotic strange meson with $J^P = 0^-$.

We gratefully acknowledge the support of the CERN management and staff and the skill and effort the technicians of our collaborating institutes. This work was made possible by the financial support of our funding agencies. This work was supported by the Excellence Cluster Universe which is funded by the Deutsche Forschungsgemeinschaft (DFG, German Research Foundation), the Excellence Cluster ORIGINS which is funded by the DFG under Germany's Excellence Strategy – EXC 2094 – 390783311, the Computational Center for Particle and Astrophysics (C2PAP), and the Leibniz Supercomputer Center

(LRZ).

Supplemental Material A: Construction of the Resonance Model

The first stage of the analysis, called partial-wave decomposition, is described in detail in Ref. [11]. The results of the partial-wave decomposition presented in that reference are identical to those presented in this paper. The second analysis stage, i.e. the resonance-model fit (RMF), presented in this paper deviates from what is presented Ref. [11] in terms of the selected set of 14 partial waves and the construction of the resonance model, while the method is the same. Therefore, we briefly describe the construction of the resonance model used in this paper in the following.

The 14 selected partial waves included in the RMF are parameterized by in total 13 resonance components, as well as a non-resonant and two background components for each wave. Table II lists these waves and the included components. In the following, we briefly summarize the parameterizations used for the individual model components. Details can be found in Ref. [11].

For the parameterization of the dynamic amplitudes of resonance components relativistic Breit-Wigner amplitudes are used [20, 42]

$$\mathcal{D}_{\text{BW}}(m; m_0, \Gamma_0) = \frac{m_0 \Gamma_0}{m_0^2 - m^2 - i m_0 \Gamma(m)}, \quad (4)$$

TABLE II: List of partial waves and model components included in the RMF. The second column lists the included resonance components. Their parameters are specified in table III. The next three columns list the parameterization for the dynamic amplitudes of the non-resonant components (NR), the model used for the $\pi^- \pi^- \pi^+$ background components and the parameterizations used for the dynamic amplitudes of the remaining background components (rem bkg). The numbers refer to the equation numbers in the text. The last two columns list the mass range for a partial wave included in the RMF.

Partial Wave	Resonances	NR	$\pi^- \pi^- \pi^+$	rem bkg	$m_{K\pi\pi}$ Range GeV/ c^2	
$0^- 0^+ \rho(770) K P$	$K(1460), K(1690),$ $K(1830)$	(10)	(11)	(13)	1.10	2.30
$1^+ 0^+ \rho(770) K S$	$\{K_1(1270), K_1(1400),\}$	(10)	(11)	(13)	1.10	2.50
$1^+ 1^+ \rho(770) K S$	$\{K'_1\}$	(10)	(11)	(14)	1.10	2.50
$2^+ 1^+ K^*(892) \pi D$	$\{K_2^*(1430)\}$	(10)	(11)	(13)	1.20	1.70
$2^+ 1^+ \rho(770) K D$		(10)	(11)	(13)	1.30	1.70
$2^- 0^+ K^*(892) \pi F$		(10)	(11)	(13)	1.60	2.00
$2^- 0^+ K_2^*(1430) \pi S$	$\{K_2(1770), K_2(1820),\}$	(7)	(11)	(14)	1.50	2.80
$2^- 0^+ \rho(770) K F$	$\{K_2(2250)\}$	(10)	(11)	(13)	1.60	2.10
$2^- 0^+ f_2(1270) K S$		(10)	(11)	(13)	1.60	2.80
$3^+ 0^+ K_3^*(1780) \pi S$	$\{K_3\}$	(10)	(11)	—	2.00	2.50
$3^+ 1^+ K_2^*(1430) \pi P$		(10)	(11)	(13)	2.00	2.50
$4^+ 1^+ K^*(892) \pi G$	$\{K_4^*(2045)\}$	(10)	(11)	(15)	1.80	2.50
$4^+ 1^+ \rho(770) K G$		(10)	(11)	(13)	1.80	2.50
$4^- 0^+ K_2^*(1430) \pi D$	K_4	(10)	(11)	(13)	2.10	2.80

with the mass-dependent width

$$\Gamma(m) = \Gamma_0 \frac{q_i(m)}{m} \frac{m_0}{q_i(m_0)} \frac{F_{L_i}^2(m)}{F_{L_i}^2(m_0)}, \quad (5)$$

which takes into account the opening of the phase space for the decay mode i in the two-body approximation. The two-body break-up momentum,

$$q_i(m) = q(m, m_1, m_2) = \frac{\sqrt{[m^2 - (m_1 + m_2)^2][m^2 - (m_1 - m_2)^2]}}{2m}, \quad (6)$$

is given by the masses m_1 and m_2 of the daughter particles. $F_{L_i}(m)$ is the centrifugal barrier factor, where L_i is the orbital angular momentum between the daughter particles.¹ Table III lists the decay modes used for the dynamic widths, the parameter limits applied in the fit, and the start parameter ranges that are used when randomly generating start parameters for the RMF.

The employed parameterization for the non-resonant components,

$$\mathcal{D}_k^{\text{NR}}(m_{K\pi\pi}; a_k, c_k) = (m_{K\pi\pi} - m_{\text{thr}})^{a_k} e^{-b(c_k) \tilde{q}_k^2(m_{K\pi\pi})}, \quad (7)$$

is inspired by Ref. [44] and was used in previous analyses, such as the COMPASS $\pi^-\pi^-\pi^+$ analysis [15].

Here, $m_{\text{thr}} = m_K + 2m_\pi$ is the kinematic threshold for $m_{K\pi\pi}$, and²

$$\tilde{q}_k(m_{K\pi\pi}) = q(m_{\text{norm}}, m_\zeta, m_\xi) \frac{m_{K\pi\pi} \mathfrak{N}_{a(k)}(m_{K\pi\pi})}{m_{\text{norm}} \mathfrak{N}_{a(k)}(m_{\text{norm}})}, \quad (8)$$

is an extension of the two-body break-up momentum of the isobar-bachelor system, which takes into account the finite width of the isobar via the phase-space integral $\mathfrak{N}_{a(k)}(m_{K\pi\pi})$ of wave a in which component k is modeled, and is hence valid also below the nominal two-body threshold (see section 6.1.2 in Ref. [11] for details). The free shape parameters are a_k and c_k , where we required the slope parameter $b(c_k)$ of the exponential in Eq. (7) to be larger than -1 (GeV/c)^{-2} by using the following parameter mapping:

$$b(c_k) = [-1 + e^{c_k}] \text{ (GeV/c)}^{-2}. \quad (9)$$

For most of the studied partial waves, a simplified version of Eq. (7) with $a_k = 0$ and $b(c_k) = b_k$, i.e.

$$\mathcal{D}_k^{\text{NR}}(m_{K\pi\pi}; b_k) = e^{-b_k \tilde{q}_k^2(m_{K\pi\pi})}, \quad (10)$$

turned out to be sufficient to describe the non-resonant components.

The $\pi^-\pi^-\pi^+$ background component is parameterized by

$$\rho_{ab}^{3\pi}(m_{K\pi\pi}, t') = \left| C^{\pi\pi\pi} \right|^2 \tilde{\rho}_{ab}^{3\pi}(m_{K\pi\pi}, t'). \quad (11)$$

¹We used the parameterization from von Hippel and Quigg [43]. See appendix D in Ref. [19] for the definition of the centrifugal-barrier factors as a function of $z = q^2(m_{K\pi\pi}, m_{h^-h^+}, m_{\xi^-})/q_R^2$, where q is the two-body break-up momentum of the $X^- \rightarrow \xi^0 \xi^-$ decay [see Eq. (6)] and $q_R = 197.3 \text{ MeV/c}$.

²We used $m_{\text{norm}} = 3 \text{ GeV/c}$.

Here, $\hat{\rho}_{ab}^{3\pi}(m_{K\pi\pi}, t')$ is the spin-density matrix of $K^-\pi^-\pi^+$ partial waves obtained from a fit to simulated $\pi^-\pi^-\pi^+$ data generated according to the result of the partial-wave decomposition of the COMPASS $\pi^-\pi^-\pi^+$ data [14]. The absolute amount of $\pi^-\pi^-\pi^+$ background in our sample is given by the free parameter $|C^{\pi\pi\pi}|^2$. This means $|C^{\pi\pi\pi}|^2$ is determined from the measured $K^-\pi^-\pi^+$ sample, while $\rho_{ab}^{\pi\pi\pi}(m_{K\pi\pi}, t')$ is completely determined by the measured $\pi^-\pi^-\pi^+$ sample.

Other incoherent background processes, such as $K^- + p \rightarrow K^- K^- K^+ + p$, also contribute to the $K^-\pi^-\pi^+$ sample. As there are no explicit models available for these processes, we parameterized them in an effective way by using the same phenomenological functional dependence on $m_{K\pi\pi}$ as used for the non-resonant components. The RMF model for the remaining background components reads

$$\hat{\mathcal{I}}_a^{\text{rem bkg}}(m_{K\pi\pi}, t') = \mathcal{K}(m_{K\pi\pi}, t') C_a^{\text{rem bkg}}(t') \mathcal{D}_{k_a}^{\text{rem bkg}}(m_{K\pi\pi}; a_{k_a}, c_{k_a}). \quad (12)$$

For most of the partial waves, we used the simplified parameterization [same as Eq. (10)]:

$$\mathcal{D}_k^{\text{rem bkg}}(m_{K\pi\pi}; b_k) = e^{-b_k \hat{q}_k^2(m_{K\pi\pi})}. \quad (13)$$

For some partial waves we used the full parameterization [same as Eq. (7)]:

$$\mathcal{D}_k^{\text{rem bkg}}(m_{K\pi\pi}; a_k, c_k) = (m_{K\pi\pi} - m_{\text{thr}})^{a_k} e^{-b(c_k) \hat{q}_k^2(m_{K\pi\pi})}. \quad (14)$$

The intensity spectrum of the $4^+ 1^+ K^*(892) \pi G$ wave exhibits an enhanced low-mass tail below $m_{K\pi\pi} \approx 2 \text{ GeV}/c^2$. To take this into account we used the following modified version of Eq. (14) to parameterize its non-resonant component:

$$\mathcal{D}_k^{\text{rem bkg}}(m_{K\pi\pi}; a_k, c_k) \rightarrow \frac{\mathcal{D}_k^{\text{rem bkg}}(m_{K\pi\pi}; a_k, c_k)}{\mathcal{K}(m_{K\pi\pi}, t')}. \quad (15)$$

TABLE III: Resonance components included in the 14 partial waves in the RMF and listed in table II. We list the fit-parameter limits and the start-parameter ranges for the mass parameters m_0 and the width parameters Γ_0 . The resonance parameters of the $K(1460)$ component were fixed in the RMF to the values measured by LHCb [2]. The resonance parameters of the $K_1(1400)$ component were fixed in the RMF to the PDG average values [1]. The last column shows the decay mode that we assumed when calculating the dynamic width of the resonance in Eq. (5). The same decay mode is used for all resonances that belong to the same J^P sector, i.e. the dominant decay channel of the dominant resonance.

Resonance	Parameter	Limits [MeV/ c^2]		Start Ranges [MeV/ c^2]		Fixed Values [MeV/ c^2]	Decay Mode for $\Gamma(m)$
$K(1460)$	m_0	—	—	—	—	1482.4	$K^*(892)\pi P$
	Γ_0	—	—	—	—	335.6	
$K(1690)$	m_0	1500	1700	1600	1650	—	$K^*(892)\pi P$
	Γ_0	10	350	150	200	—	
$K(1830)$	m_0	1800	1930	1820	1860	—	$K^*(892)\pi P$
	Γ_0	10	400	130	200	—	
$K_1(1270)$	m_0	1200	1500	1270	1290	—	$K^*(892)\pi S$
	Γ_0	50	600	80	130	—	
$K_1(1400)$	m_0	—	—	—	—	1403	$K^*(892)\pi S$
	Γ_0	—	—	—	—	174	
$K_1(1630)$	m_0	1550	2300	1600	1900	—	$K^*(892)\pi S$
	Γ_0	50	600	120	350	—	
$K_2^*(1430)$	m_0	1300	1500	1425	1435	—	$K\pi D$
	Γ_0	80	600	105	115	—	
$K_2(1770)$	m_0	1700	1790	1700	1790	—	$K^*(892)\pi P$
	Γ_0	80	600	150	200	—	
$K_2(1820)$	m_0	1800	2000	1820	1850	—	$K^*(892)\pi P$
	Γ_0	100	600	150	250	—	
$K_2(2250)$	m_0	2100	2450	2200	2280	—	$K^*(892)\pi P$
	Γ_0	50	600	150	250	—	
K_3	m_0	2100	2500	2200	2450	—	$K_2^*(1430)\pi P$
	Γ_0	100	600	100	300	—	
$K_4^*(2045)$	m_0	2000	2400	2050	2080	—	$K^*(892)\pi G$
	Γ_0	100	600	150	250	—	
K_4	m_0	2100	2650	2200	2450	—	$K^*(892)\pi F$
	Γ_0	100	600	100	300	—	

Supplemental Material B: Systematic Uncertainties

To determine the systematic uncertainties of our results for the masses and widths of the eleven strange-meson resonances we performed numerous systematic studies, which we briefly summarize in the following. Details of the performed systematic studies can be found in Ref. [11]. These studies included the event selection, in particular the final-state particle identification. We varied the stringency of the final-state particle identification requirements or removed momentum regions with a potentially imperfect modeling of the final-state particle identification in the Monte Carlo detector simulation.

We performed several studies to estimate the systematic uncertainty from the partial-wave decomposition. We estimated systematic effects from the ambiguous particle identification discussed in the main text by manually removing one of the ambiguous partial waves from the set of waves included in $\sum_{a,b}^{\text{waves}}$ in equation (1) of the main text. We also used a different approach to construct the set of waves included in $\sum_{a,b}^{\text{waves}}$ based on information field theory (see section 3 of Ref. [45] for details). This novel method uses a Bayesian regularization approach to narrow the large pool of allowed waves to those that significantly contribute to the data. This approach is different from the one used in the main analysis, and in addition imposes continuity of the partial waves in $m_{K\pi\pi}$, which is not done in the main analysis.

The systematic studies also include the resonance-model fit. We studied the use of bootstrap estimates in the χ^2 formalism. We also tested assumptions that enter the resonance-model fit, such as fixing the mass and width parameters of the $K_1(1400)$ and $K(1460)$ components, by freeing these parameters in studies. The exclusion of a second excited state K_1'' was tested by including it in a study. We tested the choice of the 14 partial waves used in the resonance-model fit by performing resonance-model fits with various subsets of these 14 partial waves.

Finally, the systematic uncertainty for a given resonance parameter is the maximum deviation from the main analysis observed in any of the above studies.³


³Some of the studies performed clearly deteriorated the quality of the data or the analysis model and produced incorrect results for a limited set of resonances, particularly for small resonances. We excluded these studies when calculating the systematic uncertainties of the resonance parameters of the resonances concerned.

Supplemental Material C: Results


This section summarizes the results of the partial-wave analysis of the reaction $K^- + p \rightarrow K^- \pi^- \pi^+ + p$. Table IV lists our results for the resonance parameters of the eleven strange-meson resonances together with the corresponding values from PDG or from individual previous measurements (see table caption for details). Figs. 3 and 4 show the intensity spectra of the 14 partial waves used in the resonance-model fit in linear and logarithmic scale, respectively. Fig. 5 shows the phases of the 14 partial waves used in the resonance-model fit in the second t' bin relative to the $1^+ 0^+ \rho(770) K S$ wave. Figs. 6 to 9 show the real and imaginary parts of the spin-density matrix elements of the 14 partial waves used in the resonance-model fit, i.e. the data that enters the resonance-model fit, and the corresponding model curves obtained from the resonance-model fit in the four t' bins.

TABLE IV: Resonance parameters as obtained from the 14-wave RMF. The first quoted uncertainties are statistical, the second systematic uncertainties. The values and uncertainties are rounded to the same precision according to the PDG rounding rules [1]. The number of significant digits is given by the total uncertainty. For the total uncertainty, we quadratically add the statistical uncertainty to the upper and lower systematic uncertainties. For comparison, the PDG averages from Ref. [1] are listed. The PDG lists more than one average value for the $K_2^*(1430)$ resonance. We list here the PDG average values for the charged $K_2^*(1430)$ decaying into the $K\pi$ final state. The PDG does not quote averages for the parameters of the $K(1630)$, $K(1830)$, and $K_4(2500)$ as there is only a single measurement for each state considered by the PDG. We quote the masses and widths from these measurement [33, 37, 38].

(a) K -like resonances

		$K(1690)/K(1630)$	$K(1830)$
	m_0 [MeV/ c^2]	$1687 \pm 10^{+2}_{-67}$	$1893 \pm 17^{+13}_{-39}$
	Γ_0 [MeV/ c^2]	$140 \pm 20^{+50}_{-50}$	$160 \pm 40^{+60}_{-80}$
PDG	m_0 [MeV/ c^2]	1629 ± 7	$1874 \pm 43^{+59}_{-115}$
	Γ_0 [MeV/ c^2]	16^{+19}_{-16}	$168 \pm 90^{+208}_{-104}$

(b) K_1 -like resonances

		$K_1(1270)$	K'_1
	m_0 [MeV/ c^2]	$1266 \pm 2^{+5}_{-9}$	$1940 \pm 10^{+90}_{-60}$
	Γ_0 [MeV/ c^2]	$88 \pm 4^{+19}_{-19}$	$430 \pm 20^{+160}_{-190}$
PDG	m_0 [MeV/ c^2]	1253 ± 7	1650 ± 50
	Γ_0 [MeV/ c^2]	90 ± 20	150 ± 50

(c) K_2 -like resonances




		$K_2(1770)$	$K_2(1820)$	$K_2(2250)$
	m_0 [MeV/ c^2]	$1714 \pm 4^{+10}_{-13}$	$1842 \pm 5^{+44}_{-19}$	$2244 \pm 10^{+18}_{-54}$
	Γ_0 [MeV/ c^2]	$152 \pm 8^{+78}_{-12}$	$273 \pm 10^{+128}_{-22}$	$260 \pm 20^{+50}_{-70}$
PDG	m_0 [MeV/ c^2]	1773 ± 8	1819 ± 12	2247 ± 17
	Γ_0 [MeV/ c^2]	186 ± 14	264 ± 34	180 ± 30

TABLE IV: Continued.

(d) K_3 - and K_4 -like resonances

		K_3	K_4
	m_0 [MeV/ c^2]	$2119 \pm 13^{+45}_{-12}$	$2210 \pm 40^{+80}_{-30}$
	Γ_0 [MeV/ c^2]	$270 \pm 30^{+40}_{-30}$	$250 \pm 70^{+50}_{-70}$
PDG	m_0 [MeV/ c^2]	2324 ± 24	2490 ± 20
	Γ_0 [MeV/ c^2]	150 ± 30	≈ 250

(e) K_J^* -like resonances

		$K_2^*(1430)$	$K_4^*(2045)$
	m_0 [MeV/ c^2]	$1430.9 \pm 1.4^{+3.1}_{-1.5}$	$2060 \pm 5^{+11}_{-3}$
	Γ_0 [MeV/ c^2]	$111 \pm 3^{+4}_{-16}$	$189 \pm 10^{+13}_{-21}$
PDG	m_0 [MeV/ c^2]	1427.3 ± 1.5	2048^{+8}_{-9}
	Γ_0 [MeV/ c^2]	100.0 ± 2.1	199^{+27}_{-19}

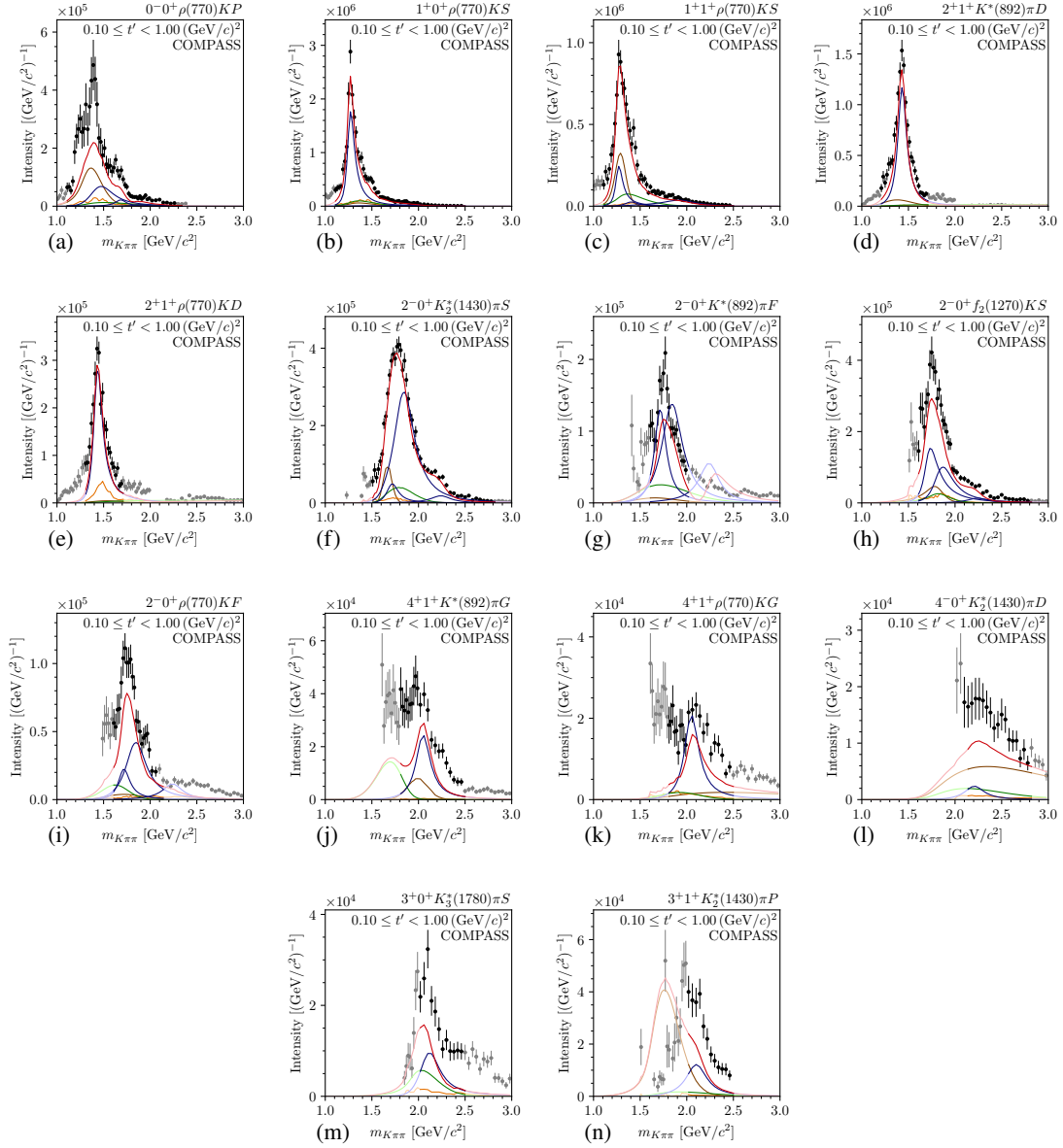


FIG. 3: t' -summed intensity spectra of the 14 partial waves used in the resonance-model fit. Data points represent the measured intensities. Curves represent the **total RMF model** (red), the individual **resonance components** (blue), the **non-resonant components** (green), the $\pi^-\pi^-\pi^+$ **background components** (orange), and the **remaining background components** (brown). Extrapolations of the model curves beyond fitted $m_{K\pi\pi}$ ranges are shown in lighter colors, grey for data points.

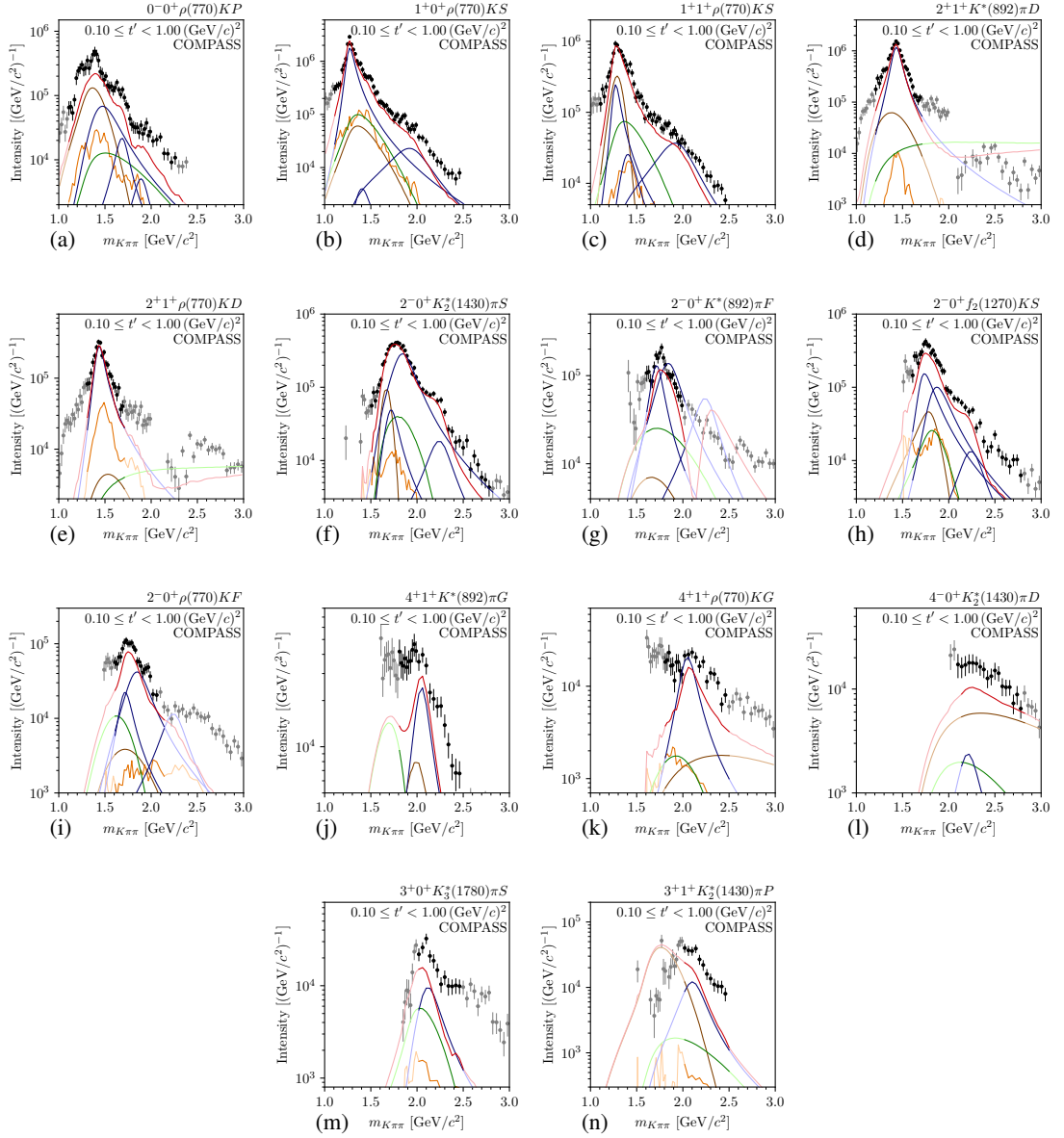


FIG. 4: Same as Fig. 3, but showing the intensity spectra in log scale.

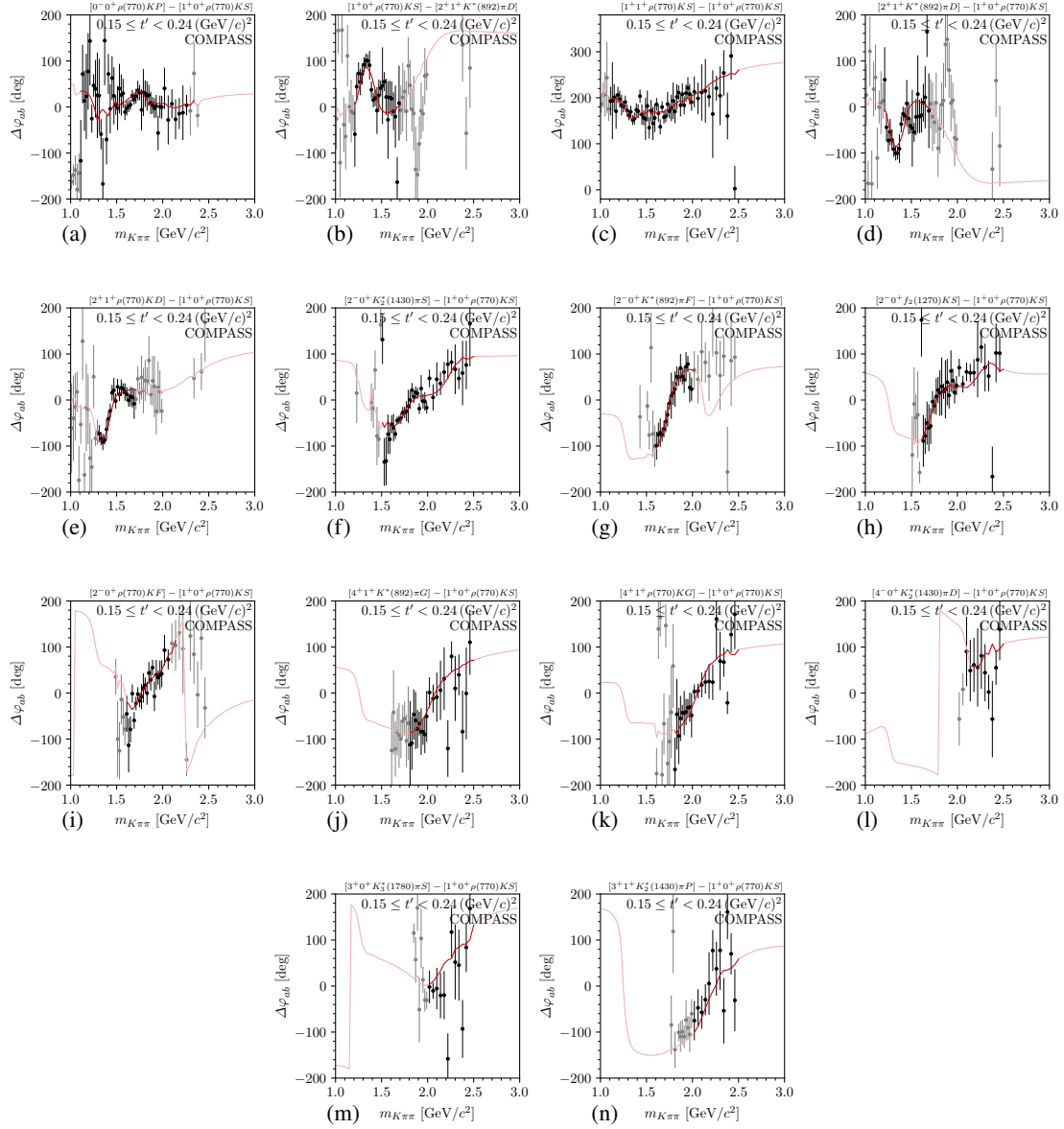


FIG. 5: Phases of the 14 partial waves used in the resonance-model fit in the second-lowest t' bin relative to the $1^+ 0^+ \rho(770) K S$ wave, except for the phase of the $1^+ 0^+ \rho(770) K S$ wave, which is shown relative to the $2^+ 1^+ K^*(892) \pi D$ wave. Same color code as in Fig. 3.

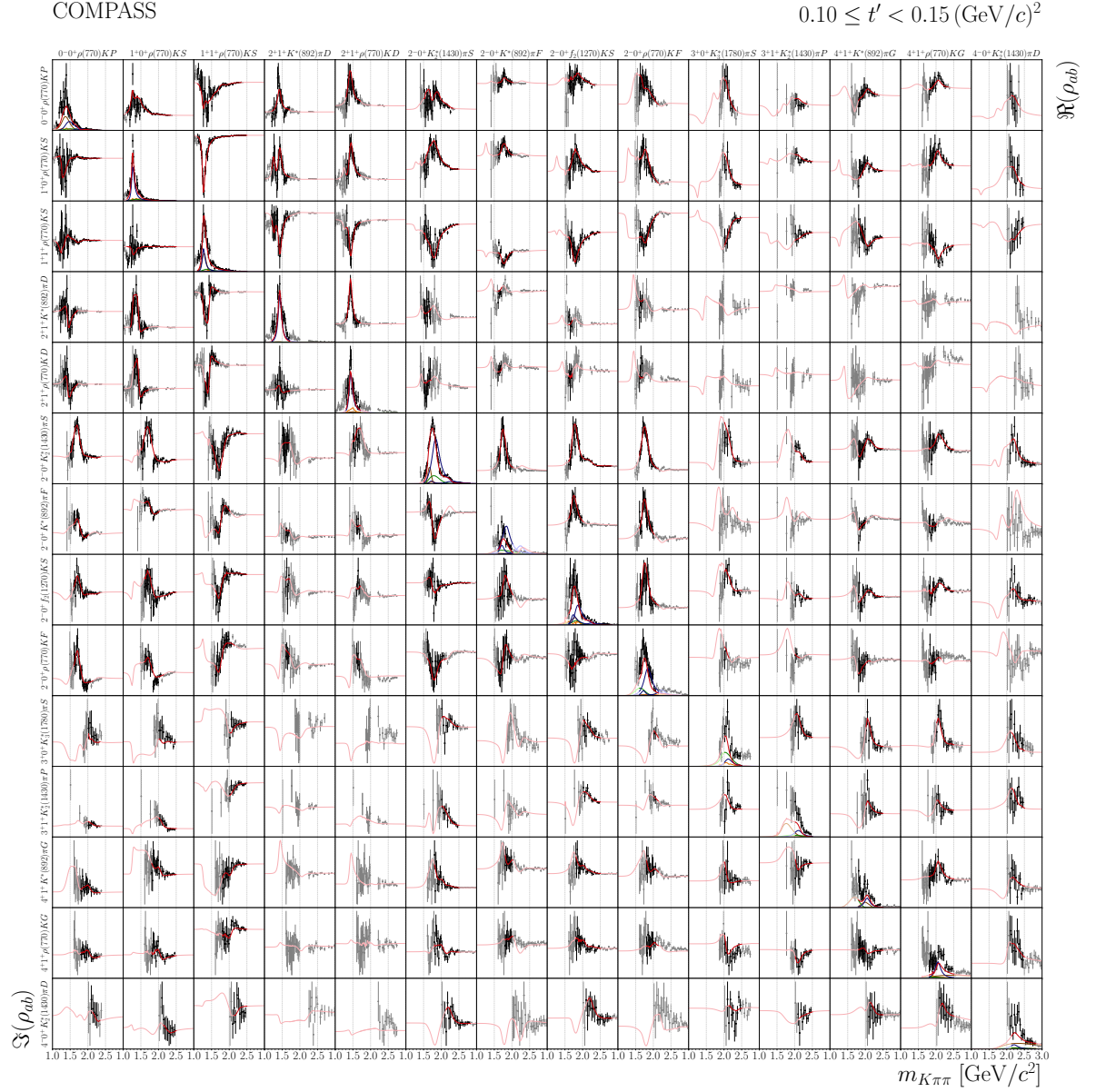


FIG. 6: (Zoom-in version for online view) Real and imaginary parts of the spin-density matrix elements as a function of $m_{K\pi\pi}$ in the lowest of the four t' bins for the 14 partial waves that were included in the resonance-model fit. The graphs on the diagonal show the intensity spectra. The upper-right and lower-left off-diagonal graphs show the real and imaginary parts, respectively, of the off-diagonal elements of the spin-density matrix. Same color code as in Fig. 3.

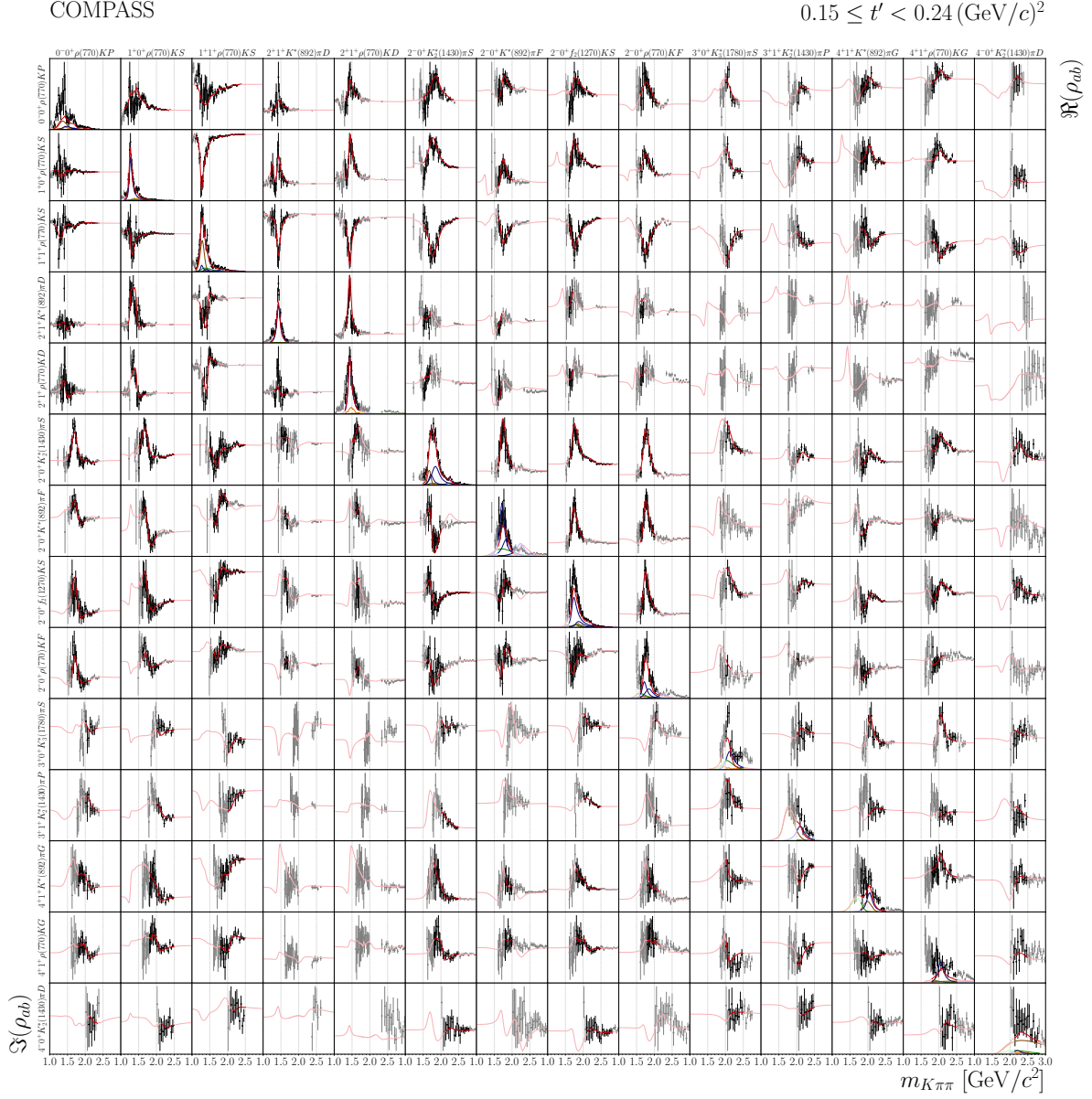
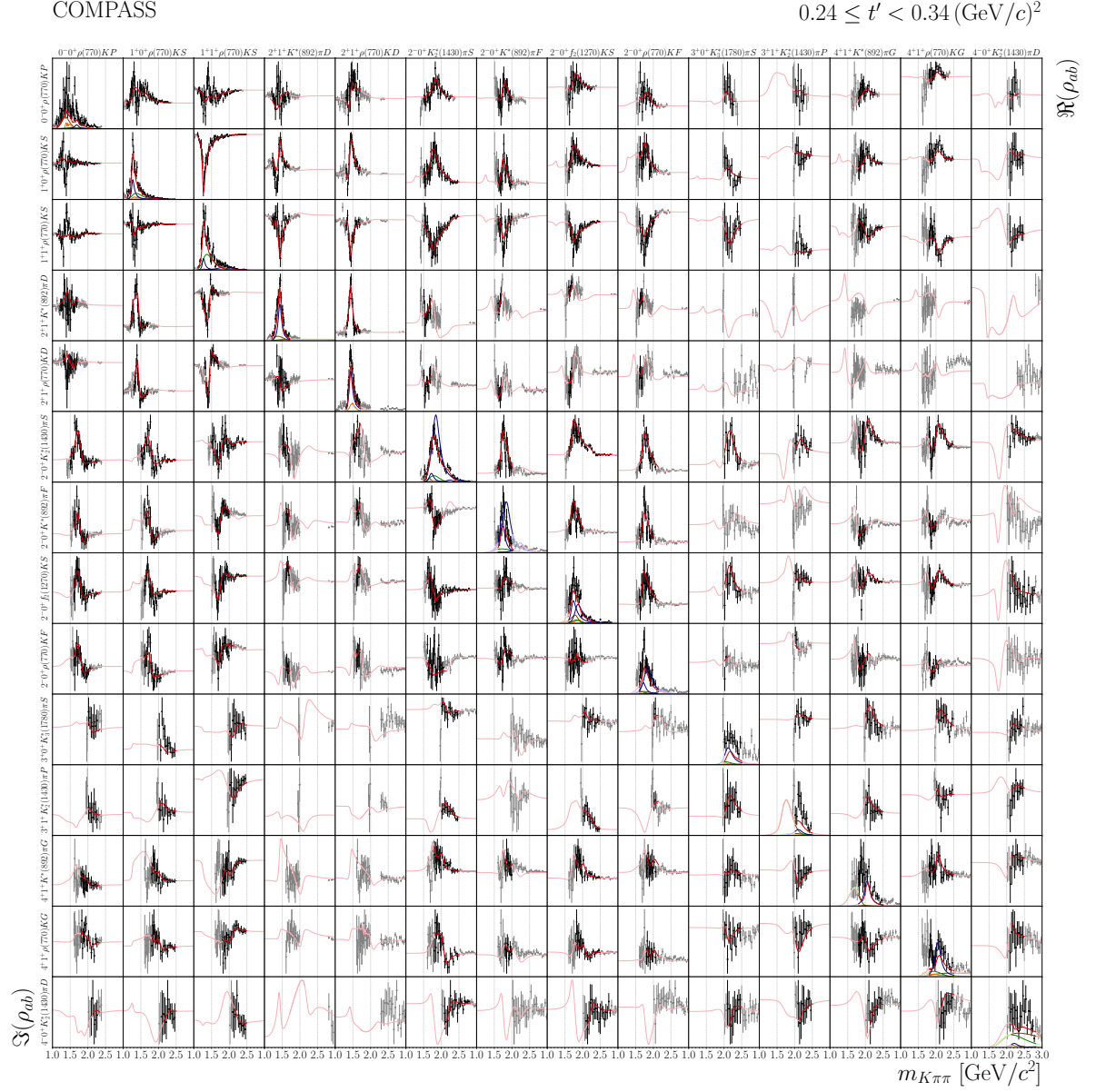
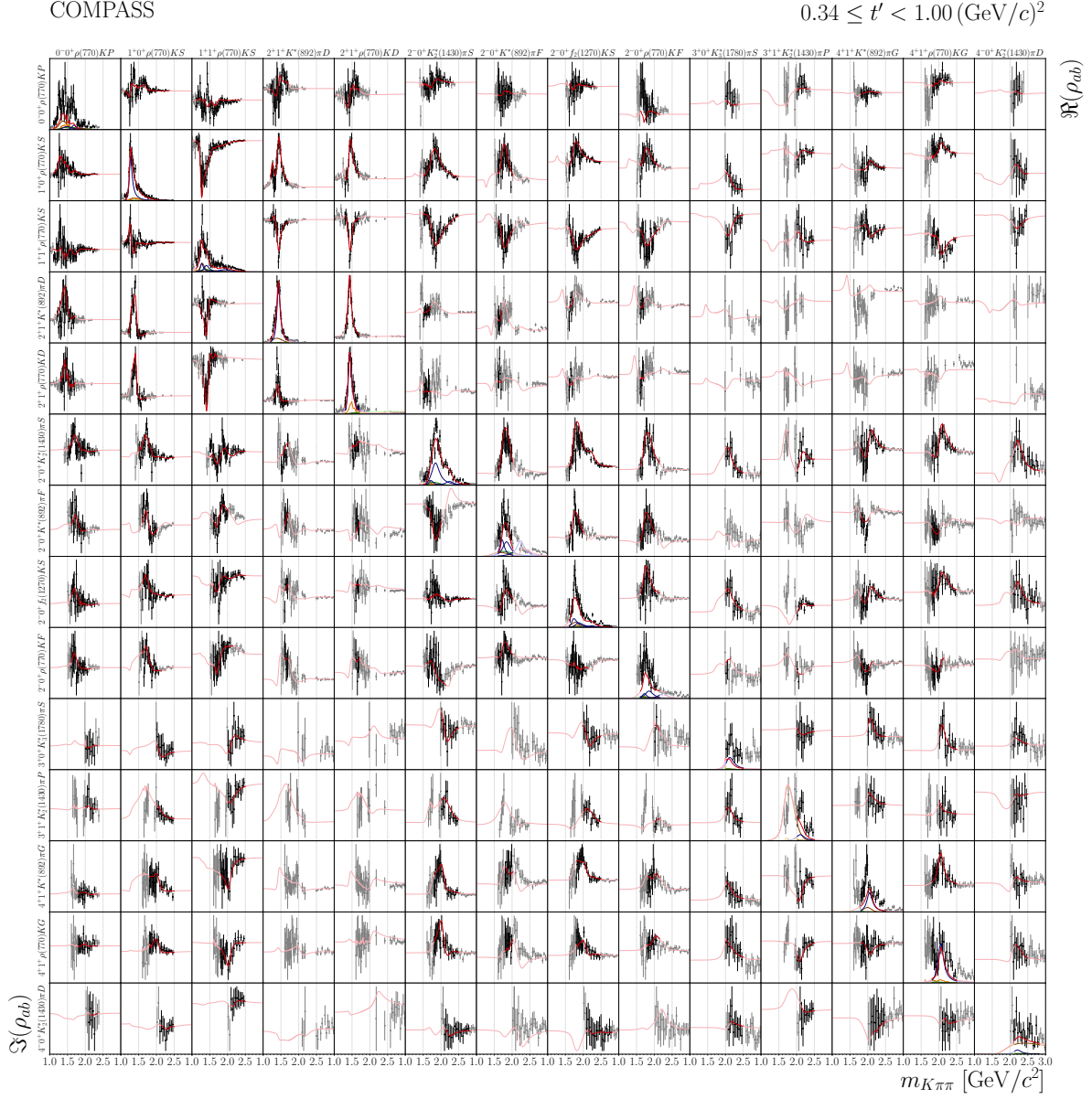


FIG. 7: Same as Fig. 6, but showing the spin-density matrix elements in the second-lowest t' bin.





References

- [1] S. Navas *et al.* (Particle Data Group), [Phys. Rev. D **110**, 030001 \(2024\)](#).
- [2] R. Aaij *et al.* (LHCb), [Eur. Phys. J. C **78**, 443 \(2018\)](#).
- [3] D. Ebert, R. N. Faustov, and V. O. Galkin, [Phys. Rev. D **79**, 114029 \(2009\)](#).
- [4] J. Oudichhya, K. Gandhi, and A. K. Rai, [Phys. Rev. D **108**, 014034 \(2023\)](#).
- [5] U. Taboada-Nieto, P. G. Ortega, D. R. Entem, F. Fernández, and J. Segovia, [Eur. Phys. J. A **59**, 40 \(2023\)](#).
- [6] C.-Q. Pang, J.-Z. Wang, X. Liu, and T. Matsuki, [Eur. Phys. J. C **77**, 861 \(2017\)](#).
- [7] S. Godfrey and N. Isgur, [Phys. Rev. D **32**, 189 \(1985\)](#).
- [8] R. Aaij *et al.* (LHCb), [Phys. Rev. Lett. **127**, 082001 \(2021\)](#).
- [9] M. G. Alexeev *et al.* (COMPASS), [Phys. Rev. D **105**, 012005 \(2022\)](#).
- [10] S. Eidelmann, T. Gutsche, C. Hanhart, R. Mitchell, and S. Spanier (Particle Data Group), [PTEP **2022**, 083C01 \(2022\)](#).
- [11] S. Wallner, [Ph.D. thesis](#), Munich, Tech. U. (2022), CERN-THESIS-2021-292.
- [12] P. Abbon *et al.* (COMPASS), [Nucl. Instrum. Meth. A **779**, 69 \(2015\)](#).
- [13] C. Daum *et al.* (ACCMOR), [Nucl. Phys. B **187**, 1 \(1981\)](#).
- [14] C. Adolph *et al.* (COMPASS), [Phys. Rev. D **95**, 032004 \(2017\)](#).
- [15] M. Aghasyan *et al.* (COMPASS), [Phys. Rev. D **98**, 092003 \(2018\)](#).
- [16] S. U. Chung and T. L. Trueman, [Phys. Rev. D **11**, 633 \(1975\)](#).
- [17] J. D. Hansen, G. T. Jones, G. Otter, and G. Rudolph, [Nucl. Phys. **B81**, 403 \(1974\)](#).
- [18] D. Herndon, P. Söding, and R. J. Cashmore, [Phys. Rev. D **11**, 3165 \(1975\)](#).
- [19] B. Ketzer, B. Grube, and D. Ryabchikov, [Prog. Part. Nucl. Phys. **113**, 103755 \(2020\)](#).
- [20] G. Breit and E. Wigner, [Phys. Rev. **49**, 519 \(1936\)](#).
- [21] Igor A. Kachaev, in *3rd International Conference on Quarks and Nuclear Physics QNP* (Bloomington, IN, U.S.A., 2004).
- [22] K. L. Au, D. Morgan, and M. R. Pennington, [Phys. Rev. D **35**, 1633 \(1987\)](#).
- [23] A. Palano and M. R. Pennington, (2017), [arXiv:1701.04881](#).
- [24] B. Efron, [Ann. Stat. **7**, 1 \(1979\)](#).
- [25] This supplemental material at [url] (2025).
- [26] R. T. Deck, [Phys. Rev. Lett. **13**, 169 \(1964\)](#).
- [27] L. Bibrzycki *et al.* (JPAC), [Eur. Phys. J. C **81**, 647 \(2021\)](#).
- [28] M. R. Atayan *et al.* (EHS/NA22), [Z. Phys. C **50**, 353 \(1991\)](#).

- [29] P. Gavillet *et al.*, [Phys. Lett. **76B**, 517 \(1978\)](#).
- [30] S. Rodebäck *et al.*, [Z. Phys. C **9**, 9 \(1981\)](#).
- [31] L. S. Geng, E. Oset, L. Roca, and J. A. Oller, [Phys. Rev. D **75**, 014017 \(2007\)](#).
- [32] D. Frame, I. Hughes, J. Lynch, P. Minto, D. McFadzean, D. Stewart, A. Thompson, R. Turnbull, and I. Wilkie, [Nucl. Phys. B **276**, 667 \(1986\)](#).
- [33] R. Aaij *et al.* (LHCb), [Phys. Rev. Lett. **118**, 022003 \(2017\)](#).
- [34] D. Aston *et al.* (LASS), [Phys. Lett. B **308**, 186 \(1993\)](#).
- [35] S. S. Wilks, [Annals Math. Statist. **9**, 60 \(1938\)](#).
- [36] T. Armstrong *et al.*, [Nucl. Phys. B **227**, 365 \(1983\)](#).
- [37] W. E. Cleland *et al.*, [Nucl. Phys. B **184**, 1 \(1981\)](#).
- [38] V. M. Karnaukhov, V. I. Moroz, and C. Coca, [Phys. Atom. Nucl. **61**, 203 \(1998\)](#).
- [39] V. M. Karnaukhov, C. Coca, and V. I. Moroz, [Phys. Atom. Nucl. **63**, 588 \(2000\)](#).
- [40] F.-K. Guo, X.-H. Liu, and S. Sakai, [Prog. Part. Nucl. Phys. **112**, 103757 \(2020\)](#).
- [41] M. G. Alexeev and Others (COMPASS), [Phys. Rev. Lett. **127**, 82501 \(2021\)](#).
- [42] M. L. Perl, *High energy hadron physics* (Wiley, 1974).
- [43] F. Von Hippel and C. Quigg, [Phys. Rev. D **5**, 624 \(1972\)](#).
- [44] N. A. Törnqvist, [Z. Phys. C **68**, 35 \(1995\)](#).
- [45] F. M. Kaspar, J. Beckers, and J. Knollmüller, [EPJ Web Conf. **291**, 02014 \(2024\)](#).

The COMPASS Collaboration

G. D. Alexeev²⁸, M. G. Alexeev^{20,19}, C. Alice^{20,19}, A. Amoroso^{20,19}, V. Andrieux³³, V. Anosov²⁸, K. Augsten⁴, W. Augustyniak²³, C. D. R. Azevedo²⁶, B. Badelek²⁵, R. Beck⁸, J. Beckers¹², Y. Bedfer⁶, J. Bernhard³⁰, F. Bradamante¹⁷, A. Bressan^{18,17}, W.-C. Chang³¹, C. Chatterjee^{17,a}, M. Chiosso^{20,19}, S.-U. Chung^{12,jj1}, A. Cicuttin^{17,16}, M. L. Crespo^{17,16}, D. D'Ago^{18,17}, S. Dalla Torre¹⁷, S. S. Dasgupta¹⁴, S. Dasgupta^{17,f}, F. Delcarro^{20,19}, I. Denisenko²⁸, O. Yu. Denisov¹⁹, S. V. Donskov^{1,29}, N. Doshita²², Ch. Dreisbach¹², W. Dünneweber^{b,b1}, R. R. Dusaev^{1,29}, D. Ecker¹², P. Faccioli²⁷, M. Faessler^{b,b1}, M. Finger^{5,†}, M. Finger jr.⁵, H. Fischer¹⁰, K. J. Flöthner⁸, W. Florian^{17,16}, J. M. Friedrich¹², V. Frolov²⁸, L.G. Garcia Ordóñez^{17,16}, O. P. Gavrichtchouk²⁸, S. Gerassimov^{29,12}, J. Giarra¹¹, D. Giordano^{20,19}, A. Grasso^{20,19}, A. Gridin²⁸, M. Grosse Perdekamp³³, B. Grube¹², M. Grüner⁸, A. Guskov²⁸, P. Haas¹², D. von Harrach¹¹, M. Hoffmann^{8,a}, N. d'Hose^{6,a}, C.-Y. Hsieh³¹, S. Ishimoto^{22,i}, A. Ivanov²⁸, T. Iwata²², V. Jary⁴, R. Joosten⁸, E. Kabuß^{11,a}, F. Kaspar¹², A. Kerbizi^{18,17}, B. Ketzer⁸, G. V. Khaustov²⁹, J. H. Koivuniemi^{7,33}, V. N. Kolosov^{1,29}, K. Kondo Horikawa²², I. Konorov^{29,12}, A. Yu. Korzenev²⁸, A. M. Kotzinian^{1,19}, O. M. Kouznetsov²⁸, A. Koval²³, F. Krinner¹², F. Kunne⁶, K. Kurek²³, R. P. Kurjata²⁴, G. Kurten^{12,e}, K. Lavickova⁴, S. Levorato¹⁷, Y.-S. Lian^{31,1}, J. Lichtenstadt¹⁵, P.-J. Lin^{32,a}, R. Longo³³, V. E. Lyubovitskij^{29,d}, A. Maggiora¹⁹, N. Makke¹⁷, G. K. Mallot^{30,10}, A. Maltsev²⁸, A. Martin^{18,17}, J. Marzec²⁴, J. Matoušek⁵, T. Matsuda²¹, C. Menezes Pires²⁷, F. Metzger⁸, W. Meyer⁷, M. Mikhasenko^{13,c}, E. Mitrofanov²⁸, D. Miura²², Y. Miyachi²², R. Molina^{17,16}, A. Moretti^{18,17}, A. Nagaytsev²⁸, D. Neyret⁶, M. Niemiec²⁵, J. Nový⁴, W.-D. Nowak¹¹, G. Nukazuka^{22,m}, A. G. Olshevsky²⁸, M. Ostrick¹¹, D. Panzner^{19,g,1}, B. Parsamyan^{1,19,30,*}, S. Paul¹², H. Pekeler⁸, J.-C. Peng³³, M. Pešek⁵, D. V. Peshekhonov²⁸, M. Pešková⁵, S. Platchkov⁶, J. Pochodzalla¹¹, V. A. Polyakov^{28,29}, C. Quintans²⁷, G. Reicherz⁷, C. Riedl³³, D. I. Ryabchikov^{29,12}, A. Rychter²⁴, A. Rymbekova²⁸, V. D. Samoylenko^{1,29}, A. Sandacz^{23,a}, S. Sarkar¹⁴, I. A. Savin^{28,†}, G. Sbrizzai¹⁷, H. Schmieden⁹, A. Selyunin²⁸, S. Seriubin²⁸, L. Sinha¹⁴, D. Spülbeck⁸, A. Srnka², M. Stolarski²³, M. Sulc³, H. Suzuki^{22,h}, S. Tessaro¹⁷, F. Tessarotto^{17,*}, A. Thiel⁸, F. Tosello¹⁹, A. Townsend^{33,k}, V. Tskhay²⁹, B. Valinoti^{17,16}, B. M. Veit¹¹, J.F.C.A. Veloso²⁶, A. Vijayakumar³³, M. Virius⁴, M. Wagner⁸, S. Wallner^{12,e,*}, K. Zaremba²⁴, M. Zavertyaev²⁹, M. Zemko⁴, E. Zemlyanichkina²⁸, M. Ziembicki²⁴

¹ A.I. Alikhanyan National Science Laboratory, 2 Alikhanyan Br. Street, 0036, Yerevan, Armenia^A

² Institute of Scientific Instruments of the CAS, 61264 Brno, Czech Republic^B

³ Technical University in Liberec, 46117 Liberec, Czech Republic^B

⁴ Czech Technical University in Prague, 16636 Prague, Czech Republic^B

⁵ Charles University, Faculty of Mathematics and Physics, 12116 Prague, Czech Republic^B

⁶ IRFU, CEA, Université Paris-Saclay, 91191 Gif-sur-Yvette, France

⁷ Universität Bochum, Institut für Experimentalphysik, 44780 Bochum, Germany^C

⁸ Universität Bonn, Helmholtz-Institut für Strahlen- und Kernphysik, 53115 Bonn, Germany^C

⁹ Universität Bonn, Physikalisches Institut, 53115 Bonn, Germany^C

¹⁰ Universität Freiburg, Physikalisches Institut, 79104 Freiburg, Germany^C

¹¹ Universität Mainz, Institut für Kernphysik, 55099 Mainz, Germany^C

¹² Technische Universität München, Physik Dept., 85748 Garching, Germany^C

¹³ Ludwig-Maximilians-Universität, 80539 München, Germany

¹⁴ Matrivani Institute of Experimental Research & Education, Calcutta-700 030, India^D

¹⁵ Tel Aviv University, School of Physics and Astronomy, 69978 Tel Aviv, Israel^E

¹⁶ Abdus Salam ICTP, 34151 Trieste, Italy

¹⁷ Trieste Section of INFN, 34127 Trieste, Italy

¹⁸ University of Trieste, Dept. of Physics, 34127 Trieste, Italy

- ¹⁹ Torino Section of INFN, 10125 Torino, Italy
²⁰ University of Torino, Dept. of Physics, 10125 Torino, Italy
²¹ University of Miyazaki, Miyazaki 889-2192, Japan^F
²² Yamagata University, Yamagata 992-8510, Japan^F
²³ National Centre for Nuclear Research, 02-093 Warsaw, Poland^G
²⁴ Warsaw University of Technology, Institute of Radioelectronics, 00-665 Warsaw, Poland^G
²⁵ University of Warsaw, Faculty of Physics, 02-093 Warsaw, Poland^G
²⁶ University of Aveiro, I3N, Dept. of Physics, 3810-193 Aveiro, Portugal^H
²⁷ LIP, 1649-003 Lisbon, Portugal^H
²⁸ Affiliated with an international laboratory covered by a cooperation agreement with CERN
²⁹ Affiliated with an institute formerly covered by a cooperation agreement with CERN
³⁰ CERN, 1211 Geneva 23, Switzerland
³¹ Academia Sinica, Institute of Physics, Taipei 11529, Taiwan^I
³² Center for High Energy and High Field Physics and Dept. of Physics, National Central University, 300 Zhongda Rd., Zhongli 320317, Taiwan^I
³³ University of Illinois at Urbana-Champaign, Dept. of Physics, Urbana, IL 61801-3080, USA^J

* Corresponding author

^a Supported by the European Union's Horizon 2020 research and innovation programme under grant agreement STRONG-2020 - No 824093

^b Retired from Ludwig-Maximilians-Universität, 80539 München, Germany

^{b1} Supported by the DFG cluster of excellence 'Origin and Structure of the Universe' (www.universe-cluster.de) (Germany)

^c Also at ORIGINS Excellence Cluster, 85748 Garching, Germany

^d Also at Institut für Theoretische Physik, Universität Tübingen, 72076 Tübingen, Germany

^e Supported by the Max Planck Institute for Physics, 85748 Garching, Germany

^f Present address: NISER, Centre for Medical and Radiation Physics, Bhubaneswar, India

^g Also at University of Eastern Piedmont, 15100 Alessandria, Italy

^{g1} Supported by the Funds for Research 2019-22 of the University of Eastern Piedmont

^h Also at Chubu University, Kasugai, Aichi 487-8501, Japan

ⁱ Also at KEK, 1-1 Oho, Tsukuba, Ibaraki 305-0801, Japan

^j Also at Dept. of Physics, Pusan National University, Busan 609-735, Republic of Korea

^{j1} Also at Physics Dept., Brookhaven National Laboratory, Upton, NY 11973, USA

^k Also at Fairmont State University, Department of Natural Sciences, 1201 Locust Ave, Fairmont, West Virginia 26554, USA

^l Also at Dept. of Physics, National Kaohsiung Normal University, Kaohsiung County 824, Taiwan

^m Also at RIKEN Nishina Center for Accelerator-Based Science, Wako, Saitama 351-0198, Japan

[†] Deceased

^A Supported by the Higher Education and Science Committee of the Republic of Armenia (Armenia)

^B Supported by MEYS, Grants LM2023040, LM2018104, LTT17018 and GAUK60121, CZ.02.01.01/00/22_008/0004632 "FORTE", co-funded by the EU and Charles University Grant PRIMUS/22/SCI/017 (Czech Republic)

^C Supported by BMBF - Bundesministerium für Bildung und Forschung (Germany)

^D Supported by B. Sen fund (India)

^E Supported by the Israel Academy of Sciences and Humanities (Israel)

^F Supported by MEXT and JSPS, Grants 18002006, 20540299, 18540281 and 26247032, the Daiko and Yamada Foundations (Japan)

^G Supported by NCN, Grant 2020/37/B/ST2/01547 (Poland)

^H Supported by FCT, Grants DOI 10.54499/CERN/FIS-PAR/0022/2019 and DOI 10.54499/CERN/FIS-PAR/0016/2021 (Portugal)

^I Supported by the Ministry of Science and Technology (Taiwan)

^J Supported by the National Science Foundation, Grant no. PHY-1506416 (USA)